Journal of
Translational Regenerative Medicine

2027. Volume 2

Research Paper

Effect of Alginate/$CaCl_2$ Treatment on the Morphology, Wettability, and Hydration of Electrospun Zein/PVP Mats

Hosein Rostamani[1], Rahil Zare[2], Omid Fakhraei[2*], Maral Emamdoost[2]

1. Department of Biomedical Engineering, School of Biomedical Engineering, Amirkabir University of Technology, Tehran, Iran.
2. Department of Biomedical Engineering, Ma.C., Islamic Azad University, Mashhad, Iran.

Use your device to scan and read the article online

Citation Rostamani H, Zar R, Fakhraei O, Emamdoost M. Effect of Alginate/$CaCl_2$ Treatment on the Morphology, Wettability, and Hydration of Electrospun Zein/PVP Mats. Journal of Translational Regenerative Medicine. 2027; 2:e256243. http://dx.doi.org/10.22034/JTRM.2.1032

http://dx.doi.org/10.22034/JTRM.2.1032

ABSTRACT

Background: Electrospun zein-poly(vinylpyrrolidone) (PVP) mats are of interest for skin wound dressing applications, but PVP's water solubility raises concerns about their interaction with water.

Methods: In this study, electrospun zein/PVP scaffolds were treated with sodium alginate followed by $CaCl_2$, and compared with an unmodified control. Zein content, total polymer concentration, and collector speed were first screened by optical microscopy. A collector speed of 500 rpm was then selected for the base scaffold because it gave a higher strain at break and more uniform fibers than the 1500-rpm speed, with similar tensile strength.

Results: Scanning electron microscopy (SEM) showed that after the alginate/$CaCl_2$ treatment, aggregates appeared at fiber crossings and pore openness was reduced. Energy-dispersive spectroscopy (EDS) detected calcium and chlorine only in the $CaCl_2$-treated group, and the water contact angle (WCA) decreased from about 76° in the base scaffold to about 42° after treatment. In PBS, the zein/PVP scaffold remained visually intact for 48 h, and its apparent water content, calculated from the initial dry weight, was 88–95% from 3 h onward, compared to that of the modified scaffold (65–79%).

Conclusion: Therefore, alginate/$CaCl_2$ treatment increased wettability but lowered the apparent water content. No cell or wet-state mechanical data were obtained. Hence, its suitability for skin tissue engineering or wound dressing use remains to be established.

Keywords: Electrospinning, Poly(vinylpyrrolidone) (PVP), Zein, Hydrogel, Wettability.

Article info:
Received: 10 Oct 2026
Accepted: 02 Jan 2027
Publish: 28 Jan 2027

*** Corresponding Author:**
Omid Fakhraei, Assistant Professor.
Address: *Department of Biomedical Engineering, Ma.C., Islamic Azad University, Mashhad, Iran.*
Phone: *+98 (936) 1351735*
E-mail: *omid.fakhraei@iau.ac.ir*

Copyright © 2027 The Author(s);
This is an open access article distributed under the terms of the Creative Commons Attribution License (CC-By-NC: https://creativecommons.org/licenses/by-nc/4.0/legalcode.en), which permits use, distribution, and reproduction in any medium, provided the original work is properly cited and is not used for commercial purposes.

Highlights

- Electrospun Zein/PVP scaffolds were treated with alginate and $CaCl_2$ in this study.
- After alginate/$CaCl_2$ treatment, aggregates formed at fiber crossings, and pores were less open.
- Alginate/$CaCl_2$ treatment lowered the WCA from about 76° to about 42° but did not increase the apparent water content in PBS
- Wet-state mechanical and cytocompatibility tests are needed before its use in skin tissue engineering

Plain Language Summary

Severe skin injuries, such as deep burns or chronic wounds, may heal more effectively with a scaffold, a thin, fabric-like mat that supports new skin cells as they grow. An effective scaffold resembles the natural fiber network surrounding cells, keeps its structure when wet, and helps maintain a moist wound environment. In this study, we produced such mats by electrospinning. The mats combined zein, a protein from corn, with poly(vinylpyrrolidone) (PVP), a polymer widely used in medicine. We then treated them with alginate, a gel-forming substance derived from seaweed, followed by calcium chloride ($CaCl_2$), which is meant to harden the gel. Collecting the fibers on a slower-rotating drum produced a more stretchable and more uniform mat. The treated mat attracted water more strongly; a water droplet spread more widely across the surface. When the mats were soaked in a salt solution that mimics body fluids, the coated mat held less water than the uncoated one. These findings matter because adding a gel coating does not automatically improve a material. The scaffold improved wetting, but the coated mat held less water after soaking. Developing better wound-care materials depends on careful testing of these mats. Before patients could benefit, the coating should be refined, and the mats should be tested for strength when wet, for loss of material during soaking, and for safety and cell attachment with human skin cells.

Introduction

The skin is the body's main interface with the environment. The skin's physical barrier, located mainly in the stratum corneum, blocks pathogens and chemical or physical insults while limiting the uncontrolled loss of water and solutes [1]. This barrier depends on adequate hydration of the stratum corneum. When water content and barrier integrity are disturbed, the skin becomes dry, rough, and scaly, a process known as the "dry skin cycle" [2, 3]. The skin is also frequently breached by trauma, surgery, burns, and chronic disease, and impaired skin wound healing affects millions of people worldwide each year [4]. Adult mammalian skin generally repairs by forming scar tissue rather than regenerating its original architecture [5, 6], which keeps the search for materials that can guide and support repair active. Skin tissue engineering addresses this need with scaffolds that temporarily substitute for the native extracellular matrix (ECM) and support cell attachment, migration, and proliferation at the injury site. Such scaffolds should mimic the fibrillar ECM, be porous enough for gas and nutrient exchange, tolerate handling and wear without losing integrity, and maintain a hydrated microenvironment at the skin interface. Electrospinning is one of the most widely used routes to this kind of structure. It produces continuous fibers with submicron- to nanometer-sized diameters, high specific surface area, and interconnected porosity; the resulting mats resemble the fibrous architecture of native ECM [7–10]. Natural and synthetic polymers can also be blended in a single spinning solution, allowing the mat's functionality to be tuned [10, 11].

Zein, the major storage protein of maize (roughly 45–50% of corn protein), is an attractive natural component for such scaffolds [12]. It is poorly soluble in water, dissolves in aqueous alcohol, and forms hydrophobic films and coatings [12]. Researchers have explored zein and zein-based materials for pharmaceutical and biomedical uses, including tissue engineering and drug delivery [12-14]. Miyoshi et al. reported ultrafine electrospun zein membranes [15]. However, protein-based electrospun fibers generally have poor mechanical properties and morphological stability in aqueous environments,

and neat zein fibers must be crosslinked to maintain their fibrous structure in physiological media [16]. Jiang et al. showed that citric acid crosslinking improved the water stability of electrospun zein fibers and increased fibroblast attachment, spreading, and proliferation compared with uncrosslinked fibers [16].

Blending zein with a hydrophilic synthetic polymer is a logical way to offset its poor wettability. Poly(vinylpyrrolidone) (PVP) is a water-soluble, biocompatible, and non-toxic Food and Drug Administration (FDA)-approved polymer and is widely used in pharmaceutical, biomedical, and cosmetic products [17]. PVP dissolves in solvents of widely different polarity [17], which facilitates co-processing with zein (soluble in aqueous alcohol [12]) in a common spinning solution. Researchers have already electrospun zein/PVP fibers for controlled release. For example, Janus zein-PVP delivered a poorly water-soluble drug in two stages [18]. However, the same water solubility that makes PVP useful means a zein/PVP mat needs a strategy to control its interaction with water if it is to be used on moist skin or wound exudate. One such strategy is to combine the fibrous mat with a hydrogel-forming phase. Alginate is a biocompatible polysaccharide that gels readily, and alginate hydrogels are widely applied in wound healing, drug delivery, and tissue engineering because they resemble tissue ECM [19]. Its chains can be ionically crosslinked with divalent cations such as Ca^{2+} [19], allowing the hydrogel to be fixed to the fibrous network under mild conditions.

In this study, we fabricated electrospun zein/PVP scaffolds and modified them with sodium alginate, followed by calcium chloride ($CaCl_2$; intended for ionic crosslinking), alongside an unmodified control. The goal was to evaluate how alginate/$CaCl_2$ treatment changes the morphology, wettability, and water uptake in phosphate-buffered saline (PBS) of the Zein/PVP scaffold. This is a preliminary materials characterization; wound dressings and skin tissue engineering scaffolds have different requirements, and without cell experiments, suitability for either is not assessed.

Materials and Methods

Materials

Zein, PVP (Mw ~1,300,000), sodium alginate, $CaCl_2$, and PBS were purchased from Sigma-Aldrich. Ethanol and distilled water were used as received.

Electrospinning

Zein and PVP were dissolved gradually in 70% ethanol until a homogeneous, transparent solution formed. Electrospinning parameters were optimized one factor at a time, and each condition was screened by electrospinning and optical microscopy of the collected deposit. First, the zein content of the polymer blend was varied at 30, 50, and 70 wt % zein of the total polymer (Z30, Z50, and Z70). Then, the total polymer concentration was varied at 15, 20, 25, and 30% w/v at Z70. Next, the collector speed was varied (250, 500, 750, and 1000 rpm) using the selected solution. We used the condition that gave a stable jet, a continuous and uniform fibrous deposit, and no droplets or discontinuities for all subsequent work. Electrospinning was carried out at 18-22 kV, 0.2-0.4 mL/h, and a nozzle-to-collector distance of 13 cm, with all other parameters held constant. For the mechanical and structural comparison, fibers were also collected at 500 and 1500 rpm. The 500-rpm scaffold was selected as the base scaffold for tensile testing and scanning electron microscopy (SEM).

Scaffold modification and sample groups

Base scaffolds were cut to identical dimensions (30×10 mm) and stored under identical conditions before modification. Two groups were prepared: unmodified zein/PVP scaffold (control) and zein/PVP/alginate scaffold. In the latter, samples were initially immersed in deionized water for about 1 min, and then were immersed in 1 %w/v sodium alginate solution for 5 min. They were gently removed to avoid tearing the coating, then transferred to 1% w/v $CaCl_2$ solution for 5 min for ionic crosslinking. After a brief wash in PBS, samples were dried at room temperature for 2 h and handled minimally throughout. The control scaffold was not exposed to any of these solutions, and no water-only or $CaCl_2$-only control was prepared.

Characterization

Chemical composition and possible interactions between components were examined by Fourier-transform infrared spectroscopy (FTIR). Spectra were recorded over 400–4000 cm^{-1} using a Jasco 6300 (Tokyo, Japan).

Fiber cross-sectional morphology, the distribution of surface deposits, and elemental composition were examined by SEM and energy-dispersive spectroscopy (EDS). The SEM was done using a TESCAN MIRA3 microscope. Samples were gold-coated beforehand, so we attributed any Au signal to sample preparation rather

than scaffold composition. The EDS was done at 15 kV and 3000× magnification, and reported as weight and atomic percent.

Wettability was assessed by water contact angle (WCA) measurements. Static contact angles were measured with a 4 µL drop of distilled water placed on the scaffold surface at 20 ˚C using a contact angle measurement apparatus (IFT-PDSA-02, Apex Technologies Co., Iran), and the image was captured immediately after deposition. Replicate drops (n=5) were measured on each sample; left and right angles were averaged for each drop, and the profile was fitted with the instrument software (Sphere Fit). Results were given as Mean±SD. We used identical droplet placement, imaging, and angle calculations for both groups.

Hydration capacity was assessed by water absorption. Initial dry weights (W_0) were recorded. Samples (n=3 per group), cut from a single scaffold, were immersed in 100 mL of PBS at room temperature and weighed, after removal of surface liquid, at 1, 2, 3, 6, 12, 24, and 48 h. Water content percentage was calculated as (Equation 1):

1. $Water\ content\ (\%)=[(W_t-W_0)/W_t]\times 100$

where W_t is the sample weight at time t, and W_0 is the dry weight. Results are given as Mean±SD.

Mechanical behavior of the base scaffolds was evaluated by tensile testing. Uniaxial tensile tests were performed on scaffolds collected at 500 and 1500 rpm using a universal testing machine (Santam Eng. Design Co. Ltd., Iran). Strip specimens (30×10 mm; gauge length=10 mm; thickness=0.026 mm) were tested at a speed of 5 mm/min on 3 specimens per group, cut from a single scaffold. We converted force–displacement data to engineering stress–strain curves, calculating stress as force divided by the apparent cross-sectional area and strain as elongation divided by the initial gauge length. Ultimate tensile strength (UTS) or maximum engineering stress as well as strain at break (strain at final specimen failure) were extracted and reported as mean±SD. We obtained mean curves by interpolating each specimen's curve onto a common strain grid and averaging point by point; we plotted them only up to the lowest strain at break among all specimens (14.9%), beyond which fewer than three curves remained. The coefficient of variation (CV) was also calculated as Equation 2:

2. $CV=(SD/mean)\times 100$.

Results

Optimization of electrospinning parameters

At a fixed total concentration of 25% w/v, the deposit depended strongly on zein content (Figure 1a). Z30 gave a dense, continuous deposit with a fine texture in which individual fibers could not be resolved (Figure 1 a_1). Optical microscopy could not determine whether this deposit was a fused fibrous mat or a film. Z50 gave sparse, curled fibers in knotted clusters, with large empty areas between them (Figure 1 a_2). Z70 gave a dense, interconnected network of continuous fibers over most of the field (Figure 1 a_3).

With the zein content fixed at Z70, the total concentration (15–30% w/v) also considerably changed the deposit (Figure 1b). At 15% w/v, the deposit mainly consisted of droplet-like features with very few fibers (Figure 1 b_1), which is consistent with electrospraying rather than fiber formation. At 20% w/v, only short, discontinuous fiber fragments and small bead-like features were observed (Figure 1b_2). At 25% w/v, a dense, continuous fibrous network without visible droplets was formed (Figure 1b_3). At 30% w/v, the fibers were coarser and more sparsely distributed, with tangled bundles and clusters, and the deposit was less uniform than at 25% w/v (Figure 1b_4). Z70 (25% w/v) therefore gave the most stable process and the best fibrous structure and was selected and used for all subsequent scaffolds.

For the selected zein-rich sample (Z70), with constant flow rate, needle-to-collector distance, applied voltage, and ambient conditions, the collector speed was first screened at 250–1000 rpm (Figure 1c). At 250 rpm, the fibers were thin, nearly straight and densely packed, with some thicker, dark fragments (Figure 1c_1). At 500 rpm, they were smooth, curved, fairly uniform in width, and well separated (Figure 1c_2). At 750 rpm, they appeared thicker and overlapped in a dense, curved network (Figure 1c_3). At 1000 rpm, only a few very wide fibers formed large loops (Figure 1c_4). The 500 rpm deposit had the most uniform fibers.

Scaffolds collected at 500 rpm and at a higher speed of 1500 rpm were then compared. SEM images (Figure 2) showed that both conditions produced interconnected fibrous networks with fibers in multiple orientations and a flattened, ribbon-like appearance. The 500-rpm scaffold appeared more homogeneous, with relatively uniform fiber widths. This scaffold was less uniform, showing variation in fiber width and localized grain-like formations along some fibers.

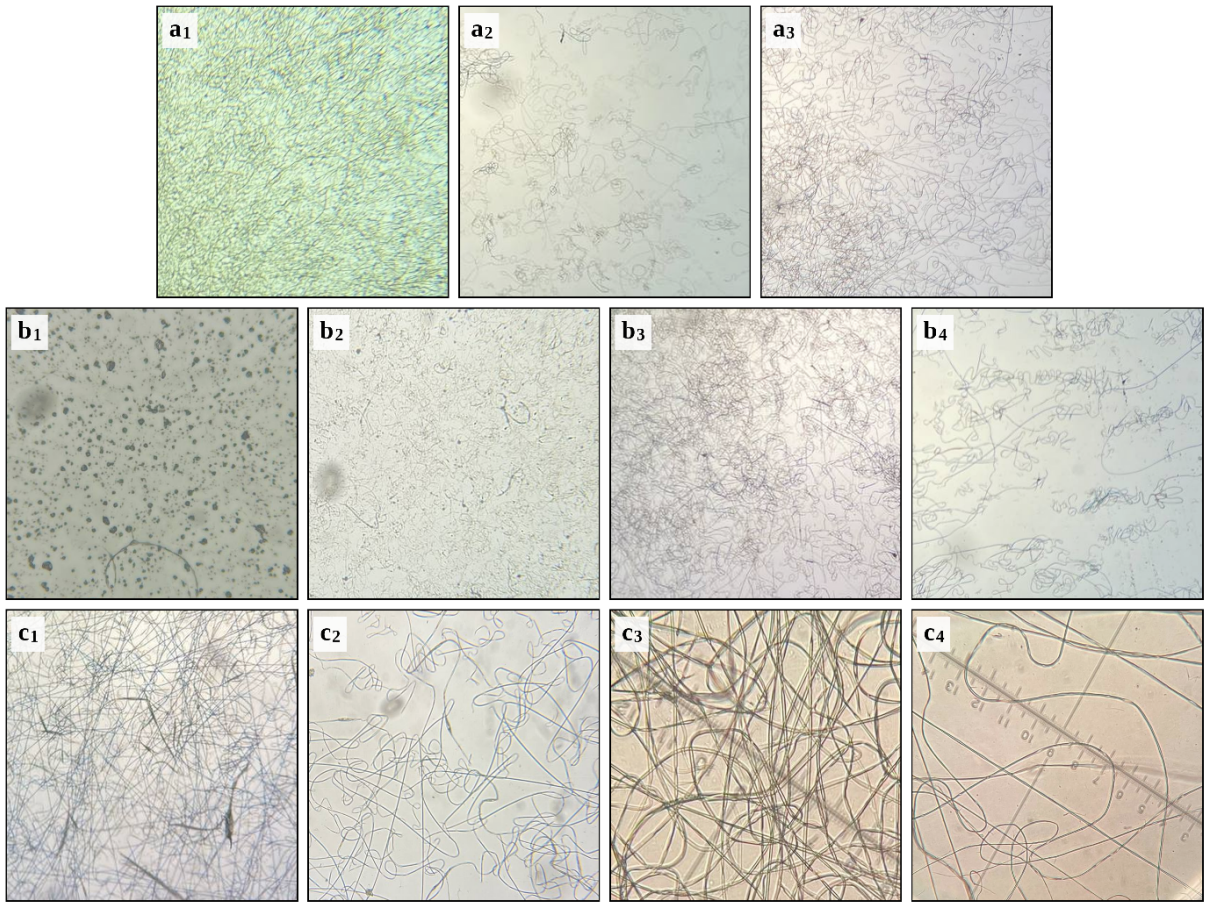


Figure 1. SEM images of the deposits collected during one-factor-at-a-time optimization of the electrospinning parameters

a) Effect of zein content at a fixed total polymer concentration of Z30 (a_1), Z50 (a_2), and Z70 (a_3), b) Effect of total polymer concentrations of 15% w/v (b_1), 20% w/v (b_2), 25% w/v (b_3), and 30% w/v (b_4) in the Z70 sample as the reference condition, c) Effect of collector speeds of 250 rpm (c_1), 500 rpm (c_2), 750 rpm (c_3), and 1000 rpm (c_4) in the Z70 sample as the reference condition

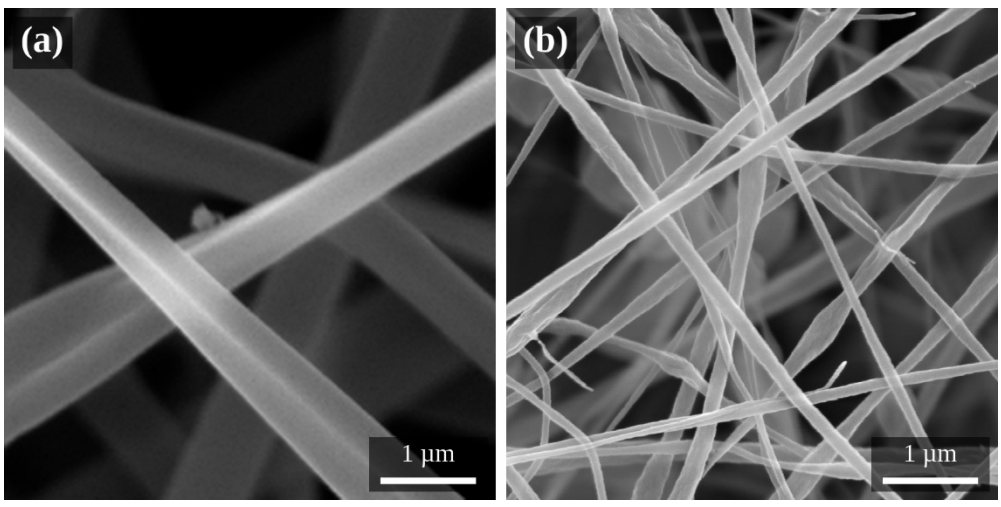


Figure 2. SEM images of scaffolds collected at 500 rpm (a) and 1500 rpm (b)

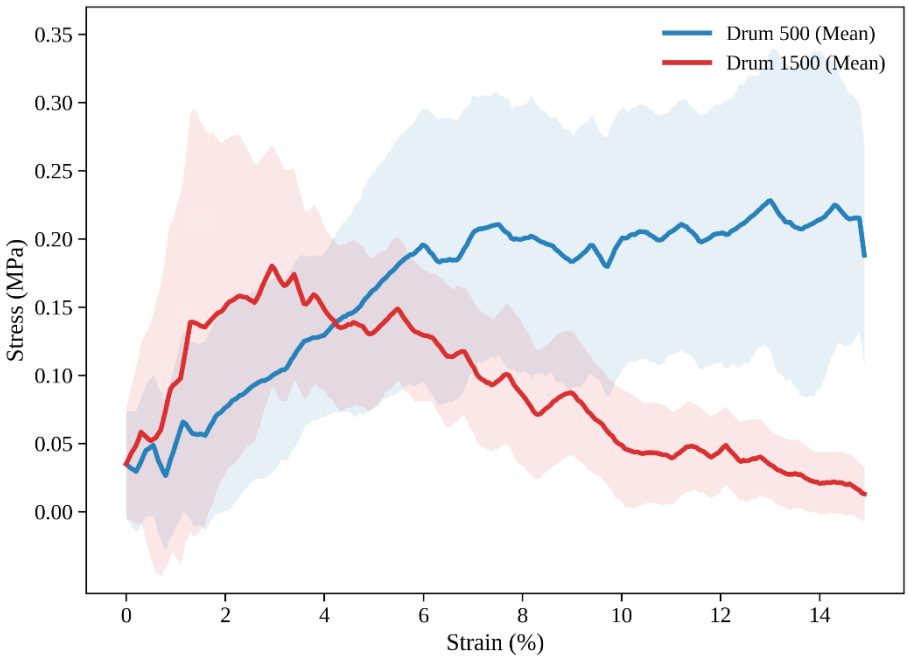


Figure 3. Mean stress–strain curves of scaffolds fabricated at drum rotation speeds of 500 and 1500 rpm (3 specimens per group, cut from one scaffold), plotted up to 14.9% strain (the lowest strain at break among the specimens)

Note: The shaded regions represent SDs.

The mean stress–strain curves from uniaxial tensile tests are shown in Figure 3. They end at 14.9% strain, the lowest strain at break among the specimens, whereas the 500-rpm specimens failed at much higher strains. Over the plotted strain range (up to ≈15%), the 1500-rpm curve peaked at about 0.15–0.18 MPa at low strain (≤5%) and then declined. The 500-rpm curve rose to about 0.2 MPa at≈6–7% strain and remained near this level. The UTS was 0.246±0.125 MPa for the 500-rpm scaffold and 0.215±0.102 MPa for the 1500-rpm scaffold (Table 1). These values overlap within one standard deviation, and the CVs were 50.7% and 47.3%, respectively. The strain at break was 47.5±6.1% for the 500-rpm scaffold and 16.8±2.6% for the 1500-rpm scaffold (Table 1), which is about 2.8 times higher at 500 rpm (CV=12.9% and 15.5%). Given 3 specimens per group as strips cut from a single scaffold, the SD reflects differences among specimens of one scaffold and not between independent fabrications. Since UTS was similar between the two groups, while strain at break and fiber uniformity were higher at 500 rpm, and 500 rpm also gave the most uniform fibers in the optical screening (Figure 1c), the 500-rpm scaffold was selected as the base scaffold for the subsequent modification and characterization.

Morphological characterization of the scaffolds

Figure 4 shows side-by-side SEM images of the two groups at identical magnification. Differences in fiber uniformity, interfiber porosity, and network continuity were visible between the groups. The zein/PVP scaffold consisted of a continuous, randomly oriented fibrous network with interconnected fibers and no noticeable discontinuities. Fiber thickness was relatively uniform, although slight variations were seen in some regions, and occasional local thickenings or small bead-like features were present. Extensive aggregates were not observed. The spaces between fibers were clearly distinguishable across the imaged areas. In cross-section, the fibers were densely interwoven and layered without distinct boundaries or delamination. Pores were distributed fairly evenly through the thickness, and no collapsed regions, cracks, or abnormal compaction were seen.

After treatment with alginate and $CaCl_2$, the scaffold retained its fibrous character but differed from the zein/PVP scaffold in network appearance. Fibers were flattened and ribbon-like in many areas, as also noted for the base scaffolds in Figure 2. Irregular, relatively coarse aggregates were present, mostly at fiber intersections and between fibers, with fine granular particles around them and on the fiber surfaces. Fibers were joined by

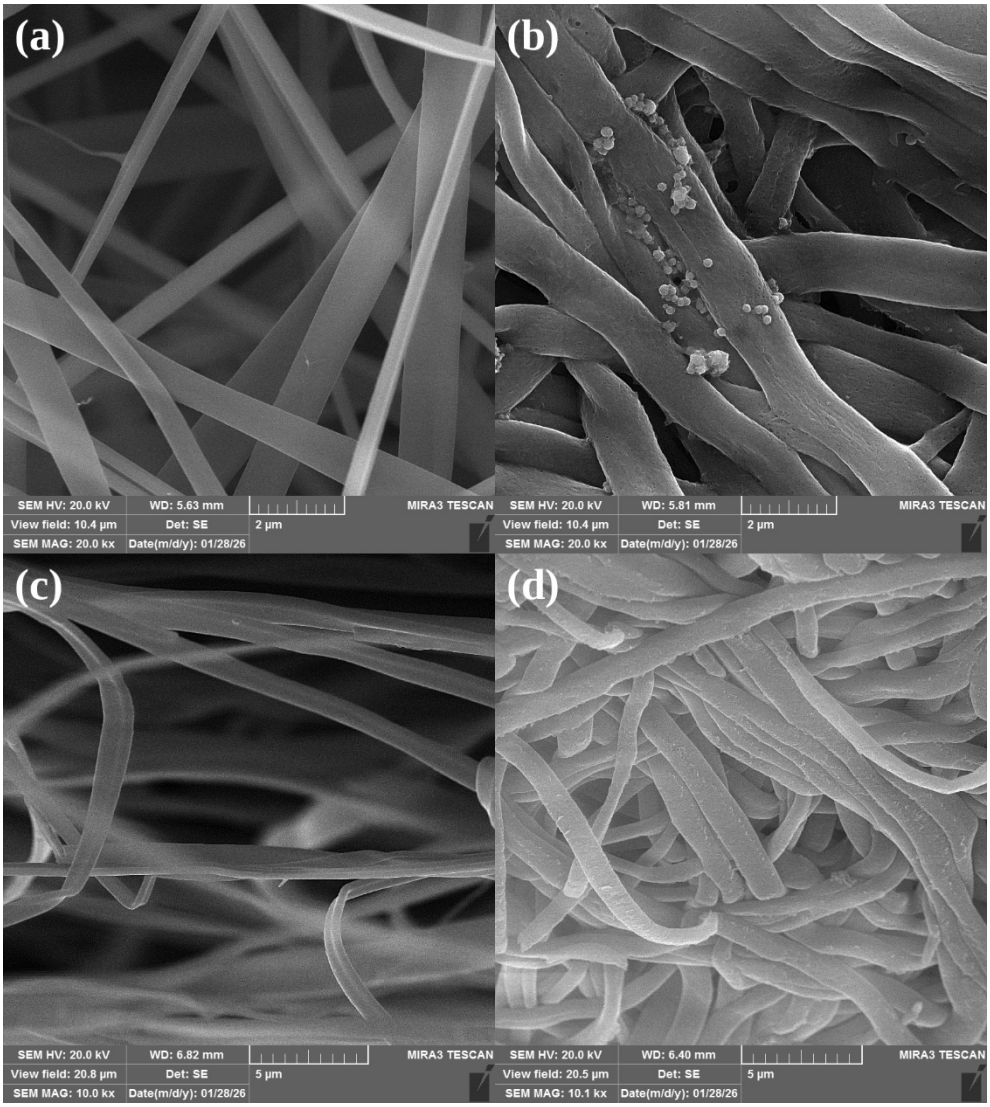


Figure 4. SEM images of the surface of scaffolds, (a) zein/PVP and (b) zein/PVP/alginate; and of the cross-sectional area of scaffolds, (c) zein/PVP and (d) zein/PVP/alginate

these deposits at some crossings, and porosity appeared locally reduced, but the fibrous framework remained recognizable. In cross-section, the fibers were flattened or folded, and local connections between fibers were visible through the depth of the scaffold. The changes were mainly at the surface and in the interfiber space; these images do not show whether material penetrated the fibers.

Overall, the alginate and $CaCl_2$ treatment procedure led to clear changes in interfiber architecture compared to the unmodified zein/PVP scaffold. These included aggregate formation, local fiber-to-fiber connections, and reduced pore openness.

Chemical and elemental characterization of the scaffolds

The FTIR spectrum of the unmodified zein/PVP scaffold was recorded in the range of 400–4000 cm^{-1} (Figure 5). A broad absorption band was centered at approximately 3310 cm^{-1}, accompanied by a weaker band at about 3072 cm^{-1}. Three bands appeared in the aliphatic C–H stretching region, at approximately 2958, 2929 and 2876 cm^{-1}. The strongest band of the spectrum was located at 1659 cm^{-1}, followed by a distinct band at approximately 1537 cm^{-1}. Further bands were detected at approximately 1440, 1290, 1230 and 1172 cm^{-1}, and in the low-wavenumber region at approximately 841, 651 and 572 cm^{-1}.

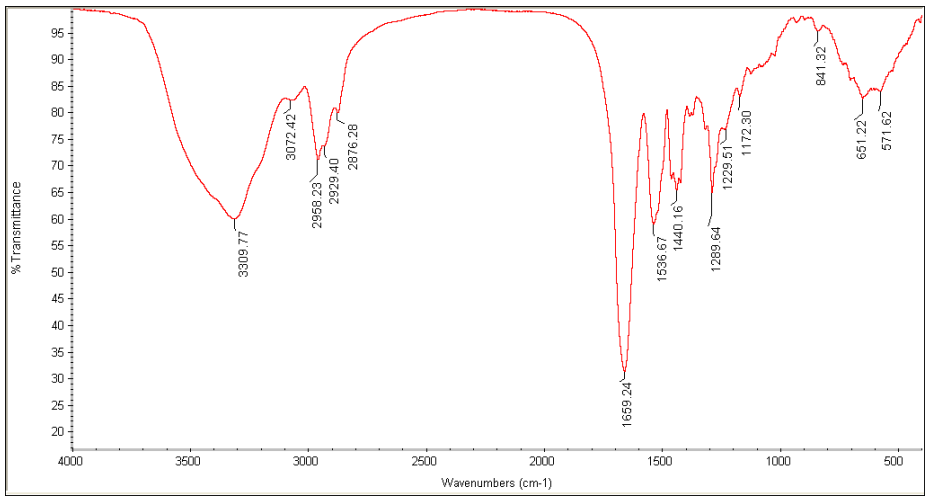


Figure 5. FTIR spectra of unmodified zein/PVP scaffold

The co-occurrence of the amide I and amide II bands with the aliphatic C–H bands aligns with FTIR spectra reported for electrospun zein [20] and PVP-containing electrospun mats [21]. The carbonyl band at 1659 cm^{-1} falls in the range where both the zein amide I and the PVP lactam C=O absorb; therefore, the contributions of the two components could not be separated in the spectrum. We recorded the spectrum for the unmodified scaffold only and used it as the reference for the base material's chemical composition.

The elemental composition of the two scaffolds was determined by EDS at an accelerating voltage of 15 kV and a magnification of ×3000. The results are given as both weight percent (wt%) and atomic percent (at %) in Table 2. The samples were gold-coated before analysis; we did not attribute any Au signal to the scaffold composition.

Carbon, nitrogen, and oxygen were the only elements detected in the zein/PVP scaffold (55.71, 22.08, and 22.20 wt%, respectively), and no calcium or chlorine was found. The same three elements were the main constituents in the zein/PVP/alginate scaffold. Compared with zein/PVP, zein/PVP/alginate had higher oxygen content (23.81 wt%) but lower carbon content (53.08 wt%). The differences in carbon, nitrogen, and oxygen content between the groups were a few percent.

Calcium and chlorine were detected only in the zein/PVP/alginate scaffold, which was treated with $CaCl_2$ (Ca: 0.35 wt%, Cl: 1.49 wt%). In this scaffold, the chlorine content exceeded the calcium content in terms of both weight and atomic percentages. Neither element was detected in the zein/PVP scaffold not exposed to $CaCl_2$ (Figure 6).

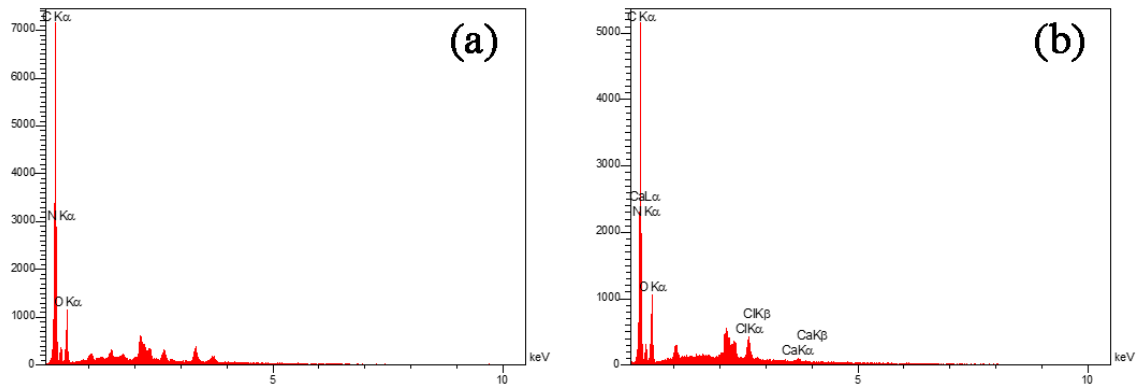


Figure 6. EDS spectra of scaffolds

a) zein/PVP, b) zein/PVP/alginate

Table 1. Tensile properties of scaffolds collected at 500 and 1500 rpm

Variables	Mean±SD	
	500 rpm	1500 rpm
UTS (MPa)	0.246±0.125	0.215±0.102
Strain at break (%)	47.5±6.1	16.8±2.6

Surface wettability of the scaffolds

The WCA measurements were performed using distilled water droplets placed on the scaffold surfaces (Figure 7). The droplet profile of each sample was analyzed, and the left, right, and average angles were recorded. The unmodified zein/PVP scaffold had a WCA of approximately 76±4°. The droplet kept a rounded, cap-shaped profile on the surface. After treatment with alginate/$CaCl_2$, the zein/PVP/alginate scaffold had a lower angle of approximately 42±4°. Compared to zein/PVP scaffold, there was a decrease of about 34°. The droplet on zein/PVP/alginate had a visibly flatter profile than on zein/PVP. For orientation, WCA values of about 40–70° are commonly cited as favorable for cell adhesion on polymeric surfaces [22], but WCA alone does not indicate biological performance.

Water uptake in PBS

The water uptake of the scaffolds was followed gravimetrically after immersion in PBS, and water content was calculated as the share of water in the total wet weight of the same specimen at each time point. It therefore cannot exceed 100% and is not directly comparable with swelling ratios normalized to dry weight. Since W_0 was used as the dry weight at each time point, any loss of material during immersion would lower the calculated value; thus, residual dry weight was not measured. Mean±SD values of water content at each time point are presented in Table 3. Both scaffolds took up a large amount of water within the first hour. Mean water contents at 1 h were 63.9% in zein/PVP and 76.4% in zein/PVP/alginate. After this time, the profiles diverged.

From 3 h onward, the zein/PVP scaffold had a higher mean water content than the zein/PVP/alginate scaffold at all time points. The 1-h water content value had a very large SD (±46.7%), showing considerable variability among replicates at that stage. For the zein/PVP/alginate scaffold, water content stayed between 75-81.9% during the first 6 h (76.4%, 81.9%, 75.0%, and 78.5% at 1, 2, 3, and 6 h). At 3 h, the Mean±SD ranges of the two scaffolds did not overlap, but they overlapped at 6 h. Because of the large SDs, especially at early time points, and the small number of replicates, group differences in the first hours should be considered indicative only. The zein/PVP scaffold showed no visible disintegration during 48 h of immersion (visual observation only).

Discussion

UTS did not separate the two collector speeds (500 and 1500 rpm); with CVs near 50% (3 specimens per group), no difference in strength can be claimed; therefore, the scaffold with 500-rpm drum rotation was selected as the base one in our study for its higher strain at break and more uniform fibers. Drum speed influences fiber orientation and stretching during collection. A study showed that, in Poly(vinylidene fluoride-co-hexafluoropropylene) (PVDF-HFP) membranes, slow rotation gave randomly deposited fibers, while fast rotation gave aligned,

Table 2. Quantitative EDS results of the scaffold groups

Element	Zein/PVP, Wt%/at%	Zein/PVP/Alginate, Wt%/at%
Carbon	55.71/61.01	53.08/59.10
Nitrogen	22.08/20.74	21.27/20.31
Oxygen	22.20/18.25	23.81/19.91
Calcium	–	1.49/0.56
Chlorine	–	0.35/0.12

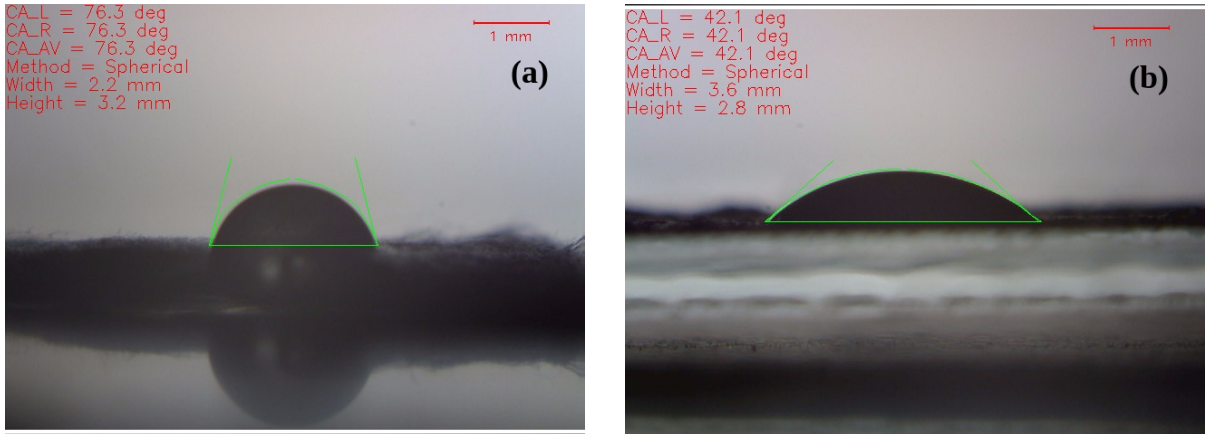


Figure 7. WCA measurement

a) zein/PVP, b) zein/PVP/alginate

thinner fibers and a much stiffer response along the alignment direction [23]. There is no clear consistency between our study and this study at either speed here, and because linear collector velocity depends on drum diameter, rpm values cannot be transferred between studies. The lower strain at break at 1500 rpm may relate to the less uniform fibers and grain-like features seen in SEM images, or to fiber stretching during collection. We did not quantify fiber diameter and orientation; therefore, the comparison of uniformity is qualitative. The choice of 500 rpm is therefore practical. Each factor was varied at each time point; one representative micrograph was shown per condition, and interactions between zein content, concentration, and collector speed were not examined; therefore, Z70 (25% w/v) was the best tested condition but not necessarily an optimum condition.

The base scaffold had low absolute strength, consistent with other reports that zein-based electrospun mats are mechanically weak and unstable in water [16, 24]. For example, drug-loaded zein/PVP/polyethylene oxide nanofibers reached about 1.5 MPa with an elongation at break of about 2.6% [25]. The mats in our study were weaker but considerably more extensible, although differences in composition, thickness, test conditions, and cross-sectional area estimates make these comparisons approximate. The amide II band in the FTIR spectrum at about 1537 cm^{-1} can be assigned to zein because PVP is a tertiary lactam without N–H groups and is not expected to contribute here, consistent with other studies [20, 21]. Because the amide I band at 1659 cm^{-1} overlaps with the PVP carbonyl, we cannot assign it to interactions between the two polymers.

The SEM changes after alginate/$CaCl_2$ treatment (aggregates at crossings, reduced pore openness) may reflect the alginate solution wetting the mat, gelling on contact with Ca^{2+}, and drawing fibers together as it dried,

Table 3. Water content (%) of the scaffolds in PBS at different time points

Time (h)	Mean±SD	
	Zein/PVP	Zein/PVP/Alginate
1	63.9±46.7	76.4±12.9
2	82.7±6.5	81.9±8.0
3	89.3±1.9	75.0±2.6
6	88.8±9.1	78.5±5.1
12	90.0±2.4	75.2±10.7
24	95.2±5.8	72.0±6.5
48	88.1±3.6	65.0±5.8

but the deposits were not identified as alginate. Contact with the aqueous solutions alone may also have contributed, since PVP is water-soluble [17] and fibers could soften and fuse on contact with them. No water-only or $CaCl_2$-only control was prepared; hence, these contributions cannot be separated, and the morphological changes cannot be attributed to alginate. Reduced pore openness matters for a skin scaffold because it can limit gas exchange and cell infiltration. On the other hand, fiber-to-fiber joints could have helped a wet mat hold together, but this was not tested.

In our study, EDS detected Ca and Cl only in the zein/PVP/alginate scaffold, indicating that part of the $CaCl_2$ treatment remained after processing. According to the egg-box model, Ca^{2+} interacts with carboxylate groups of alginate [26]; therefore, calcium bound this way does not require chloride, whereas the measured atomic Cl:Ca ratio of about 4.7 exceeds the expected ratio of 2 for $CaCl_2$ residue alone. Therefore, some chloride was not paired with the detected calcium. Residual NaCl formed by ion exchange may be the possible reason, but sodium was not detected in the study scaffolds. Elemental analysis of alginate gels can separate adsorbed salt from ions incorporated in junction zones [27]. The analysis in our study was done on one area per sample at ×3000 magnification without replicates, so the amounts detected (0.35 wt% Ca) may partly reflect local sampling. Nitrogen contents (21–22 wt%) were higher than the expected nominal composition of zein and PVP, suggesting limited quantitative accuracy of EDS on rough, porous fibrous samples; therefore, we did not interpret the few-percent differences in carbon, nitrogen, and oxygen content between the two scaffold groups. Comparative FTIR or X-ray photoelectron spectroscopy (XPS) of the modified scaffold and the raw materials may be needed to establish crosslinking.

The lower WCA of the zein/PVP/alginate scaffold is consistent with a hydrophilic alginate layer [19] on the fibers and between them, but the deposits were not identified as alginate and no water-only control was included. Static angles, however, depend on surface roughness and measurement conditions [22], and also on a porous, absorbent mat; a droplet that wicks in can give a low apparent angle without the surface being much more hydrophilic. The 40–70° range cited for cell adhesion [22] comes from general surface-testing literature, not from skin cells on electrospun mats, and adhesion also depends on protein adsorption, roughness, and stiffness; hence, the lower WCA alone does not show suitable biological performance. The zein/PVP scaffold reached a higher water content, as expected for a mat of a water-soluble polymer with interconnected pores [17], and it showed no visible disintegration over 48 h. This is encouraging, since neat zein fibers usually need crosslinking to maintain their structure in aqueous media [16], but this was only a visual observation; residual dry weight was not measured in our study. At 6 h, the mean water contents corresponded to a wet weight of about 4.7 times the dry weight in zein/PVP/alginate and 9 times in zein/PVP. The modified scaffold's lower water content is consistent with the SEM findings, because filled interfiber spaces and an alginate layer (if crosslinked) could limit capillary uptake and swelling, but no experimental tests were done in this study. The calculation also assumed that no dry weight was lost in PBS; PVP is water-soluble [17], and the coating may lose components, which would reduce the calculated water content; therefore, we cannot separate water uptake from mass loss here. Whether lower uptake is an advantage depends on the use. A moist wound environment is considered beneficial for healing, and dressings (including alginate-based ones) are used to control wound healing [28, 29]. For a scaffold intended to hydrate dry skin, a higher capacity may be preferred, whereas for exuding wounds, excessive swelling is undesirable. The test in our study measured water uptake only in excess PBS, and no evaporation or drying test was performed; therefore, these data describe water uptake and not moisture retention.

Ionotropic alginate networks are reversible physical gels [30, 31], and PBS contains phosphate and monovalent ions that compete with Ca^{2+}. Thus, a coating that retains calcium only partially could be vulnerable in PBS; we did not assess the coating's stability in this study, and the lower water content should not be considered as evidence of degradation. Although the coating improved wettability and adds a hydrogel-forming component, based on the present study data, the zein/PVP/alginate scaffold cannot be regarded as an improvement in the base scaffold. Whether a different coating or crosslinking protocol could maintain the wettability gain while preserving mechanical integrity in PBS remains to be tested.

As a limitation of this study, tensile tests and FTIR covered only the base scaffolds; therefore, we did not evaluate the effect of coating on mechanical performance in the dry or wet state. Also, we considered 3 specimens from a single scaffold per group for tensile and water-uptake assessments; hence, reproducibility across independent fabrications was not assessed; pore size was not quantified, residual dry weight and time-resolved images during immersion were not recorded, and no cell work was done. The last point matters because residual chloride and calcium could affect cell response.

Conclusion

In this study, electrospun Zein/PVP scaffolds were treated with sodium alginate followed by $CaCl_2$. They were compared with the unmodified scaffold. A collector speed of 500 rpm produced a more extensible, more uniform base mat (strain at break 47.5% versus 16.8%), although its tensile strength was low and did not differ from the 1500-rpm speed. The unmodified scaffold showed no visible disintegration in PBS over 48 h, and its calculated water content was 88–95% of the wet mass from 3 h onward. Alginate/$CaCl_2$ treatment lowered the WCA from about 76° to about 42° and was followed by deposits on the fiber surfaces and in the interfiber spaces. It was also accompanied by aggregates at fiber crossings and reduced pore openness, but without a water-only control, these changes cannot be attributed to alginate. EDS showed Ca and Cl in the $CaCl_2$-treated scaffold, but this does not by itself show that the alginate was crosslinked. The alginate/$CaCl_2$ treatment improved wettability but gave a lower apparent water content in PBS, which cannot be attributed to lower uptake or to reduced stability, because residual dry weight was not measured in this study. Its effect on mechanical performance was not evaluated because tensile tests were limited to the unmodified base scaffolds. The material characterization does not establish suitability for skin tissue engineering or wound dressing use, which require optimization of the coating and crosslinking conditions, residual dry weight measurement with time-lapse imaging in PBS, XPS of the scaffolds, replication of EDS after a defined washing step, wet-state tensile tests of coated and uncoated scaffolds, water vapor transmission and dehydration measurements, and cytocompatibility tests, such as cell attachment and spreading, with skin fibroblasts and keratinocytes.

Ethical Considerations

Compliance with ethical guidelines

There were no ethical considerations to be considered in this research.

Funding

This research did not receive any grant from funding agencies in the public, commercial, or non-profit sectors.

Authors' contributions

Conceptualization: Hosein Rostamani; Methodology and investigation: Rahil Zare; Data analysis: Maral Emamdoost; Writing: Omid Fakhraei and Hosein Rostamani.

Conflict of interest

The authors declared no conflict of interest.

Acknowledgments

The authors would like to thank Alireza Gomroki for his valuable insights.

References

[1] Banaee Mofakham E, Hesaraki S, Pazouki M, Esfandeh M. Developing a novel electrospun nanofibrous dressing containing nanostructured lipid carriers and moringa oleifera leaf extract for epidermolysis bullosa wounds. Journal of Translational Regenerative Medicine. 2026; 1:e246024. [DOI:10.32598/JTRM.1.1016]

[2] Rawlings AV, Harding CR. Moisturization and skin barrier function. Dermatologic Therapy. 2004; 17(Suppl 1):43-8. [DOI:10.1111/j.1396-0296.2004.04S1005.x] [PMID]

[3] Rawlings AV, Matts PJ. Stratum corneum moisturization at the molecular level: An update in relation to the dry skin cycle. The Journal of Investigative Dermatology. 2005; 124(6):1099-110. [DOI:10.1111/j.1523-1747.2005.23726.x] [PMID]

[4] Eming SA, Martin P, Tomic-Canic M. Wound repair and regeneration: Mechanisms, signaling, and translation. Science Translational Medicine. 2014; 6(265):265sr6. [DOI:10.1126/scitranslmed.3009337] [PMID]

[5] Takeo M, Lee W, Ito M. Wound healing and skin regeneration. Cold Spring Harbor Perspectives in Medicine. 2015; 5(1):a023267. [DOI:10.1101/cshperspect.a023267] [PMID]

[6] Gurtner GC, Werner S, Barrandon Y, Longaker MT. Wound repair and regeneration. Nature. 2008; 453(7193):314-21. [DOI:10.1038/nature07039] [PMID]

[7] Fakhraei O, Rostamani H, Aliebrahim Nosh Abad A, Valizadeh S, Bakhshayeshi MM, Rafienia M. Enhanced biological properties of polyvinyl alcohol-polycaprolactone/hyaluronic acid-coated electrospun scaffolds for articular cartilage regeneration. Journal of Biomaterials Science. Polymer Edition. 2025; 36(15):2187-215. [DOI:10.1080/09205063.2025.2492462] [PMID]

[8] Rostamani H, Rafienia M, Fakhraei O, Poursamar A, Mahdizadeh N. Electrospun Polyurethane/Alginate-Chondroitin Sulfate Scaffolds for Chondrogenesis. Materials Chemistry and Physics. 2026 Sep 16:133138. [DOI:10.1016/j.matchemphys.2026.133138]

[9] Agarwal S, Wendorff JH, Greiner A. Use of electrospinning technique for biomedical applications. Polymer. 2008; 49(26):5603-21. [DOI:10.1016/j.polymer.2008.09.014]

[10] Sharifianjazi F, Esmaeilkhanian A, Nafchi MR, Bazli L, Pourhakkak P, Rostamani H, et al. Manufacturing of nanocomposites by electrospinning. In: Myasoedova VV, Thomas S, Maria HJ, editors. Chemical Physics of Polymer Nanocomposites: Processing, Morphology, Structure, Ther-

modynamics, Rheology. Weinheim: Wiley-VCH GmbH; 2024. [DOI:10.1002/9783527837021.ch4]

[11] Rostamani H, Firouzfar S, Fakhraei O, Nakhaei N, Shahraki N, Rafienia M. Dual-functionalized electrospun PLA/PCL blend scaffolds as bioactive platforms for osteochondral tissue engineering. International Journal of Polymeric Materials and Polymeric Biomaterials. 2026; 75(11-14):1389-405. [DOI:10.1080/00914037.2026.2690024]

[12] Corradini E, Curti PS, Meniqueti AB, Martins AF, Rubira AF, Muniz EC. Recent advances in food-packing, pharmaceutical and biomedical applications of zein and zein-based materials. International Journal of Molecular Sciences. 2014; 15(12):22438-70. [DOI:10.3390/ijms151222438] [PMID]

[13] Demir M, Ramos-Rivera L, Silva R, Nazhat SN, Boccaccini AR. Zein-based composites in biomedical applications. Journal of Biomedical Materials Research. Part A. 2017; 105(6):1656-65. [DOI:10.1002/jbm.a.36040] [PMID]

[14] Reddy N, Yang Y. Potential of plant proteins for medical applications. Trends in Biotechnology. 2011; 29(10):490-8. [DOI:10.1016/j.tibtech.2011.05.003] [PMID]

[15] Miyoshi T, Toyohara K, Minematsu H. Preparation of ultrafine fibrous zein membranes via electrospinning. Polymer International. 2005; 54(8):1187-90. [DOI:10.1002/pi.1829]

[16] Jiang Q, Reddy N, Yang Y. Cytocompatible cross-linking of electrospun zein fibers for the development of water-stable tissue engineering scaffolds. Acta Biomaterialia. 2010; 6(10):4042-51. [DOI:10.1016/j.actbio.2010.04.024] [PMID]

[17] Franco P, De Marco I. The use of poly(N-vinyl pyrrolidone) in the delivery of drugs: A review. Polymers (Basel). 2020; 12(5):1114. [DOI:10.3390/polym12051114] [PMID]

[18] Wang M, Li D, Li J, Li S, Chen Z, Yu DG, et al. Electrospun Janus zein-PVP nanofibers provide a two-stage controlled release of poorly water-soluble drugs. Materials & Design. 2020; 196:109075. [DOI:10.1016/j.matdes.2020.109075]

[19] Lee KY, Mooney DJ. Alginate: Properties and biomedical applications. Progress in Polymer Science. 2012; 37(1):106-26. [DOI:10.1016/j.progpolymsci.2011.06.003] [PMID]

[20] Wang S, Li J, Wang P, Zhang M, Liu S, Wang R, et al. Improvement in the sustained-release performance of electrospun zein nanofibers via crosslinking using glutaraldehyde vapors. Foods. 2024; 13(10):1583. [DOI:10.3390/foods13101583] [PMID]

[21] Rahmani F, Ziyadi H, Baghali M, Luo H, Ramakrishna S. Electrospun PVP/PVA nanofiber mat as a novel potential transdermal drug-delivery system for buprenorphine. Applied Sciences. 2021; 11(6):2779. [DOI:10.3390/app11062779]

[22] Liber-Kneć A, Łagan S. Surface Testing of Dental Biomaterials-Determination of Contact Angle and Surface Free Energy. Materials (Basel). 2021; 14(11):2716. [DOI:10.3390/ma14112716] [PMID]

[23] Maurya AK, Mias E, Schoeller J, Collings IE, Rossi RM, Dommann A, et al. Understanding multiscale structure-property correlations in PVDF-HFP electrospun fiber membranes by SAXS and WAXS. Nanoscale Advances. 2021; 4(2):491-501. [DOI:10.1039/D1NA00503K] [PMID]

[24] Martin A, Cai J, Schaedel AL, van der Plas M, Malmsten M, Rades T, et al. Zein-polycaprolactone core-shell nanofibers for wound healing. International Journal of Pharmaceutics. 2022; 621:121809. [DOI:10.1016/j.ijpharm.2022.121809] [PMID]

[25] Saar S, Tuğcu-Demiröz FN, Acartürk F. Electrospun tenofovir/emtricitabine-zein nanofibers for pre-exposure prophylaxis platform against HIV through vaginal delivery. ACS Omega. 2025; 10(46):56302-18. [DOI:10.1021/acsomega.5c08217] [PMID]

[26] Paoletti S, Donati I. Comparative insights into the fundamental steps underlying gelation of plant and algal ionic polysaccharides: Pectate and alginate. Gels (Basel, Switzerland). 2022; 8(12):784. [DOI:10.3390/gels8120784] [PMID]

[27] Zueva OS, Khair T, Kazantseva MA, Latypova L, Zuev YF. Ions-induced alginate gelation according to elemental analysis and a combinatorial approach. International Journal of Molecular Sciences. 2023; 24(22):16201. [DOI:10.3390/ijms242216201] [PMID]

[28] Nuutila K, Eriksson E. Moist wound healing with commonly available dressings. Advances in Wound Care. 2021; 10(12):685-98. [DOI:10.1089/wound.2020.1232] [PMID]

[29] Cao Y, Cong H, Yu B, Shen Y. A review on the synthesis and development of alginate hydrogels for wound therapy. Journal of Materials Chemistry. B. 2023; 11(13):2801-29. [DOI:10.1039/d2tb02808e] [PMID]

[30] Makarova AO, Derkach SR, Khair T, Kazantseva MA, Zuev YF, Zueva OS. Ion-induced polysaccharide gelation: Peculiarities of alginate egg-box association with different divalent cations. Polymers (Basel). 2023; 15(5):1243. [DOI:10.3390/polym15051243] [PMID]

[31] Rostamani H, Fakhraei O, Kelidari N, Toosizadeh Khorasani F. Improving biological and mechanical properties of bioprinted PCL-alginate-chondrocyte scaffolds for patellofemoral cartilage tissue regeneration. Journal of Biomaterials Science. Polymer edition. 2024; 35(16):2549-69. [DOI:10.1080/09205063.2024.2385182] [PMID]